Thermal property characterisation of additively manufactured copper as a function of sintering time

Roy Urwin[1] *& Bradley D.* Bock[1*]

[1]Clean Energy Research Group, Department of Mechanical and Aeronautical Engineering, University of Pretoria, South Africa

Abstract. Recent advancements now allow for high thermal conductivity metals such as copper to be additively manufactured and will allow for the applications of the technology to be broadened in the field of heat transfer. In this study, copper samples were additively manufactured using bound powder extrusion (BPE) and thermally sintered and then characterised in terms of thermal conductivity and specific heat capacity. The sintering hold time was varied to determine the influence between the resulting change in porosity and the measured properties. For this study it was found that porosity is a function of sintering hold time and varies between 44 to 25% for a sintering hold time of between 0 to 20 hours. Specific heat capacity was found to not be a function of sintering hold time, but samples tested had a slightly lower specific heat capacity value than expected ranging from 380 to 360 J/kg/K. The copper thermal conductivity was significantly reduced by the process to between 35 to 73 W/mK. It was found to be a function of sintering hold time, and some empirical models can estimate this property relatively well.

1 Introduction

Advancements in the additive manufacturing field now allow for high thermal conductivity metals to be manufactured with relative ease. This creates an opportunity for the heat transfer industry to create more complex geometries than commercial subtractive manufacturing allows [1] that are optimized for heat transfer. However, the properties of parts produced through additive manufacturing are different to traditionally manufactured parts. For example, additive manufactured parts generally produce parts with an increased surface roughness [2], which will need to be factored into designs. In some fields, such as pool boiling, increased surface roughness is typically a positive, as it increases the number of nucleation sites present on a given material and thus enhances the pool boiling heat transfer coefficient [3]. In applications where flow is present, such as convective heat transfer, the increased roughness will increase pressure drop and thus operational losses [4], a factor that design engineers need to consider.

A technology gaining traction for the printing of high thermal conductivity metals is Bound Powder Extrusion (BPE) [5]. This procedure uses a specialized filament that mixes polymer binding matrix and metal powder. This filament is then used to print components in the same way as the classic Fused Filament Fabrication (FFF) processes used for polymers, but after which the part is then debound and sintered, which removes the polymer binder and fuses the metal powder, thus creating the solid metal component [6]. The polymer binder is

* Corresponding author: bradley.bock@up.ac.za

typically removed through either heat or chemical means, while the metal is typically fused through thermal sintering. The BPE methods allows for high conductivity metals to be additively manufactured without encountering the issue seen in other methods. Powder Bed Fusion for example commonly struggles to print copper due to the extremely high thermal conductivity of copper, as the heat from the laser is dissipated throughout the entire metal powder layer, preventing a component from being printed [7].

In terms of thermal conductivity, the open literature reports a large variation in thermal conductivity for metals manufactured using BPE. Ebrahimi and Ju [8] reported a maximum thermal conductivity of approximately 90 W/mK during their research. It was reported in this research that the polymer binder within the copper material interfered with the thermal conductivity thus reducing it [8]. Bock *et al.* however, found that the thermal conductivity of the copper can be as high as 185 W/mK [9]. This study also conducted experiments to determine the porosity and specific heat of these parts with findings of 20-27% and 0.37 J/kgK respectively [9]. However, Bock *et al.* used a higher sintering temperature and left the samples in the kiln for longer when compared to Ebrahimi and Ju, which is likely why their results differ.

Ebrahimi and Ju also performed porosity test and reported most of the copper samples tested had a porosity of 30-40%. However, they found that the porosity of a sintered part can be as high as 55%. However, these values will differ based on sintering time as the longer the part is sintered the lower the expected porosity [8]. Urwin and Bock [10] confirm Ebrahimi and Ju's finding as porosity values form that study reported porosity of 35% and a volume shrinkage of 26%.

Montes-Ramirez et al. [11] while only measuring porosity and density noted preventing impurities from entering the part during printing process was of great importance for metals printed with BPE. Ebrahimi and Ju [8] and Bock *et al.* [9] confirm this as during both their testing impurities and/or oxidation was found in the parts after sintering.

Ultrasonic-assisted pressureless sintering (UAPS) was performed on parts produced by BPE by Singh and Pandey [12]. This was done as UAPS has been used in previous research to improve the material properties of metals. It was that the thermal conductivity of additively manufactured copper produced in this study was approximately 280 W/mK. This high thermal conductivity was cause by large reductions in surface porosity [12]. In the study a combination of UAPS and increased sintering temperatures results in a 5.4% surface porosity. However, this study determined porosity using microscopic inspection which may have introduced errors into the calculation.

Considering other additive manufacturing methods of metals besides BPE shows similar trends of reduced thermal and density properties due to porosity, while rougher surface finishes are obtained. A binder jet printing studies by Thang, *et al.* [13] found that copper components attained a density of between 76 and 86 % of the density of pure copper, whereas Constantina, *et al.* [14] achieved a density of 95 % and a volume shrinkage of between 35 and 45%. Constantina, et al. [14] also found that parts tested and a surface roughness (R_a) of 18 µm. Urwin and Bock [10] found that the surface roughness value is highest on surfaces with layer lines with a surface roughness (R_a) of 16 µm. However, areas without layer line have a lower surface roughness (R_a) of 8 µm.

Wei, *et al.* [15] performed thermal conductivity studies on various metal powders for during powder bed additive manufacturing such as stainless steel and titanium. They found that the thermal conductivity of the metal powders was reduced to roughly 1% of the bulk material value. However, they found that the thermal conductivity of the powders could be

improved by introducing various gases such as helium during sintering [15]. They concluded that the introduction of such gases during the manufacturing process could improve the thermal conductivity of the manufactured component.

Vincent, *et al.* [16] investigated sintered copper powder and associated properties like porosity. They identified that thermal conductivity is a function of porosity with porosity of test samples varying form 0-25%. Their research found that thermal conductivity decreases in a linear fashion after a porosity of 6% is exceeded and reduced to 240 W/mK at 25%. Additionally they found that the grain pattern within the copper microstructure also influenced thermal conductivity with spherical grains resulting in the lowest overall value [16].

As can be seen, quantitative data regarding the actual material properties of additively manufactured metals using BPE is sparse and somewhat inconsistent at times, particularly for properties relevant to heat transfer, such as thermal conductivity and specific heat capacity. From literature there is also several underlying factors which change the material properties of metal produced using BPE, with porosity, impurities and oxidation the main contributors based on literature. This poses a serious challenge for engineers as these properties are fundamental to allow for accurate design of heat transfer devices.

Therefore, this paper seeks to expand the information on the resulting properties of BPE parts produced with thermal sintering. Properties relevant to heat transfer designers will be focussed on, namely specific heat capacity and thermal conductivity, while porosity, volume and mass reduction will be investigated to better understand the geometry of the final parts. Properties will be investigated across a range of sintering hold times to determine if any relationship between the properties investigated and sintering hold time exists to allow designers a simple method of modifying the material properties to better suit their designs.

2 Methodology

2.1 Samples

The samples printed in this research were 10 mm cubes and cylinders with a diameter of 30 mm and a height 10 mm. The cylinders, however, were upscaled across all dimensions by 10% to compensate for volume shrinkage during sintering. As such the printed cylinders have a diameter of 33 mm and a height of 11 mm. The cubes were not upscaled.

The reason for upscaling the cylinders was that the thermal conductivity setup required a sample with a diameter of approximately 30mm. Thus, the cylinders were upscaled so that they had an approximate diameter of 30 mm after sintering.

2.2 Additive manufacturing process

2.2.1 Printing process

The samples were printed using a Fused Filament Fabrication (FFF) style 3D printer, where filament composed of copper powder and a polymer/PLA matrix was extruded to produce the part. An Ender 3 PRO 3D printer was used to print the samples, with the only modification to the printer being that the nozzle of the printer was changed from a brass 0.4

mm nozzle to a hardened steel 0.6 mm nozzle as per filament manufacturer's (The Virtual Foundry) recommendation [17]. While the manufacturer recommends the use of a 'Filawarmer' to make the filament more flexible and make printing easier [17]. It was found that this device was not needed in this research. The filament was printed with a nozzle temperature of 235 °C, bed temperature of 60 °C and a print speed of 30 mm/s.

2.2.2 Debinding and sintering

The following process was followed to debind and sinter the 3D printed samples.

The debinding process

The crucible was filled to the halfway mark with refractory (aluminum oxide (AlO_3)) and compacted into the crucible. Then the part was placed into the crucible and pressed into the refractory. More refractory was then added to cover the part and compacted again. Finally, the crucible was placed into the kiln and debound using The Virtual Foundry's method [18].

- Heat the kiln to 482°C at a rate of 56°C per hour.
- Keep the kiln at the temperature for 4 hours.
- Allow the kiln and the part to cool to room temperature.

After which the part was removed from the crucible and the refractory salvaged for later use.

The sintering process

For sintering the same process for preparing the sample is used as in the debinding process. However, in this case the refractory is Talc powder.

The remaining space in the crucible was then filled with sintering carbon as per The Virtual Foundry recommendations [19].

The reason that sintering carbon is applied is to prevent oxidation from occurring during the sintering process [19]. Due to the high temperature of the sintering process the risk of oxidation is extremely high and if oxidation were to occur it could possibly ruin the part rendering it unless. Finally, the crucible was placed into the kiln and sintered using The Virtual Foundry's method [18].

- Heat the kiln to a temperature of 1052°C at a rate of 111 °C per hour.
- This temperature was then maintained for different lengths of time (referred to as hold time) with a minimum of two cubes and one cylinder being exposed to each hold time value. These hold times were 0, 2.5, 5, 10, 20 hours.

Post sintering cooling.

After the sintering process is complete, the parts are cooled. How this is done will influence the final material properties and thus serves as an effective heat treatment process.

In this study, after sintering, the part was left in the kiln and both were allowed to cool to room temperature, after which the part was removed from the crucible.

2.2.3 Copper filament used

The filament was composed of 90% copper powder and 10% polymer matrix by weight [17], with a density of between 4500-4700 kg/m^3. Since the density of copper is approximately 8940 kg/m^3 [20] and PLA be 1240 kg/m^3 [21], this means a volume fraction of PLA of only around 37%.

2.3 Porosity

The porosity (ϕ) of the samples can be determined using the Archimedes method [22]. This method measures the mass of a porous material in both air and submerged in a liquid medium. Equation (1) is then used to determine the density of the porous material and by extension its porosity.

However, due to the porous nature of the samples, it was necessary to seal their surfaces to prevent water absorption during testing. Therefore, they were sealed using paraffin wax and the Archimedes equation modified to remove the density contribution of the sealant this is shown in equation (3).

$$\rho_{Archimedes} = \frac{m_{dry}}{m_{dry} - m_{wet}} \rho_{liquid} \tag{1}$$

$$\rho_{sample} = \frac{m_{dry}}{\frac{m_{total}}{\rho_{Archimedes}} - \frac{m_{sealeant}}{\rho_{sealant}}} \tag{2}$$

$$\phi = \left(1 - \frac{\rho_{sample}}{\rho_{reference}}\right) 100 \tag{3}$$

- $\rho_{Archimedes}$: The density of the sample obtained from Archimedes method ($\frac{kg}{m^3}$)
- m_{dry}: Mass of the sample measured in air (kg)
- m_{wet}: Mass of sample submerged in the liquid medium (kg)
- ρ_{liquid} is the density of the liquid medium in this case water (kg)
- m_{total}: Mass of the sample plus the mass of the sealant measured in air (kg)
- $m_{sealeant}$: Mass of sealant in air (kg)
- $\rho_{sealant}$: Density of sealant ($\frac{kg}{m^3}$)
- $\rho_{reference}$: Density of the material with zero porosity in this case copper ($\frac{kg}{m^3}$)

This equations combined with the uncertainty of the mass (0.01 g) was used to calculate the uncertainty using the "Law of the propagation of uncertainty" [23] shown in equation 4 to determine the uncertainty of equation (4). The uncertainty of the porosity was determined to be less than 5%.

$$\Delta y^2 = \sum_{i=1}^{N} \left(\frac{dy}{dx_i}\right)^2 \Delta x_i^2 \tag{4}$$

- Δy: The uncertainty of the function
- $\frac{dy}{dx_i}$: The partial derivative of the function y with respect to variable x_i
- Δx_i The uncertainty associated with variable x_i.

2.4 Volume and mass reduction

The volume and mass reduction during sintering were calculated using the mass and the overall dimensions of the sample. The mass of the sample was obtained using an ADAM HCB 1002 digital scale (error of 0.01 g) and the overall dimensions from the Archimedes method using the density of the sample and the mass of the sample.

The uncertainty of both values was found to be less than 5% for all samples

2.5 Specific heat capacity

Fig. ***1*** shows the setup for the specific heat capacity experiments. This experiment is a variation of coffee cup calorimetry. To perform the experiment, a known mass of water was added to the calorimeter and some time was allowed for the calorimeter and the water to reach the same uniform temperature. This temperature was then noted.

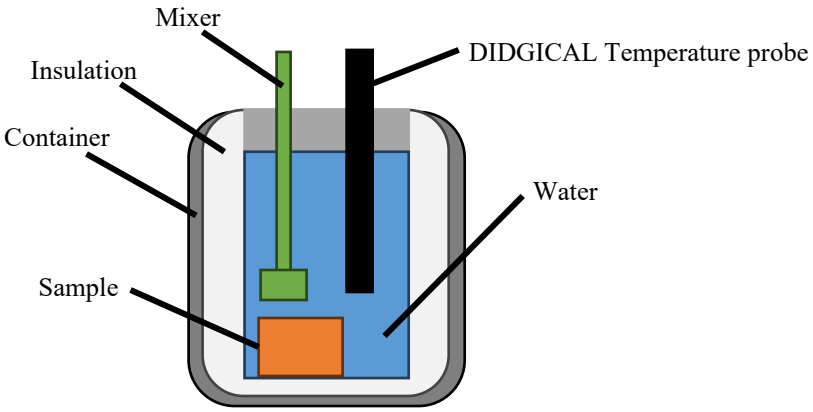

Fig. 1. Schematic of the specific heat capacity setup.

After which the mass of the sample was then measured before the test. The sample tested was then placed into a kiln heated to 90 C°. Time was allowed for both the kiln and the sample to reach a steady state operating temperature, which was then noted.

Once steady state had been reached the sample was then transferred to the calorimeter and both the sample and the water were allowed to reach a uniform temperature with the mixer being used to ensure even temperature distribution. After which the final uniform temperature was then taken. Equation (5). below was then used to determine the sample specific heat capacity. The uncertainty for this equation was less than 3.5%.

$$c_{p,sample} = \frac{c_{p,water} m_{water} \left(T_{final} - T_{water}\right)}{m_{sample} \left(T_{sample} - T_{final}\right)} \tag{5}$$

- m_{water}: Mass of water (kg)
- m_{sample}: Mass of the sample (kg)
- $c_{p,water}$: Specific heat capacity of water $(\frac{J}{kgK})$
- T_{sample}: Initial temperature of the water (C^o)

- T_{water}: Initial temperature of the water (C^o)
- T_{final}: Final temperature of both the sample and the water (C^o)

2.6 Thermal conductivity

Fig. ***2*** shows the experimental setup used to determine the thermal conductivity of the samples. This research made use of the comparative method to determine thermal conductivity which evaluates the thermal conductivity given the behavior of a reference sample [24].

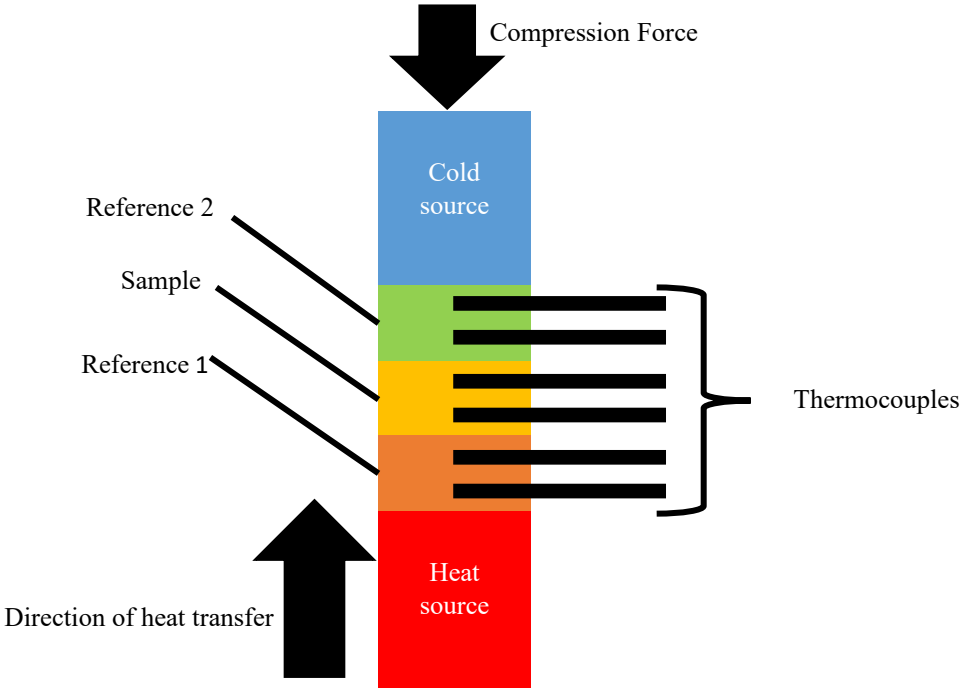

Fig. 2. Schematic of the thermal conductivity setup.

As can be seen in Fig. ***2*** reference samples were placed in the setup one above and below the actual sample. This arrangement was then placed between a cold source and the heat source. The heat source in this experiment comprised of three ceramic heating cartilages which were connected to a DC power source to output constant power. These probes were then inserted into a copper heating block which made-up the heat source. This heater block was a cylinder 30mm in diameter therefore to ensure good contact surface area all samples tested were approximately 30mm in diameter. The cold source was comprised of two water-cooled heat sinks which were connected to a constant temperature bath set to 5 C°. All surfaces were polished to a 3-micron surface finish as best as possible and treated with an application of thermal paste to limit the contact resistance. Once this arrangement was set up a compression force was applied to the entire experimental setup thus allowing good contact surface area. Equation (6) below was then used to determine the thermal conductivity of the samples. This experiment yielded less than 2% uncertainty.

$$k_{sample} = \frac{D_{ref}^2 L_{samplek} k_{ref}(\Delta T_{ref})}{D_{sample}^2 L_{ref}(\Delta T_{sample})} \quad (6)$$

- ΔT_{ref}: Temperature change across the reference (C^o)
- ΔT_{sample}: Temperature change across the sample (C^o)
- D_{ref}: Diameter of the reference (m)
- D_{sample}: Diameter of the sample (m)
- L_{ref}: Distance between the thermocouples in the reference (m)
- L_{sample}: Distance between the thermocouples in the sample (m)
- k_{ref}: Thermal conductivity of the reference ($\frac{W}{mK}$)

3 Results

3.1 Porosity

Porosity reduces as sintering hold time increases, as can be seen in Fig. ***3***. A maximum porosity of between 35-45% is achieved at a sintering hold time of 0 hours, while a minimum value of between 30-25% is achieved at a sintering hold time of 20 hours. However, from Fig. ***3*** it appears that the porosity plateaus at the 30-25% mark at a hold time of 10 hours using this method.

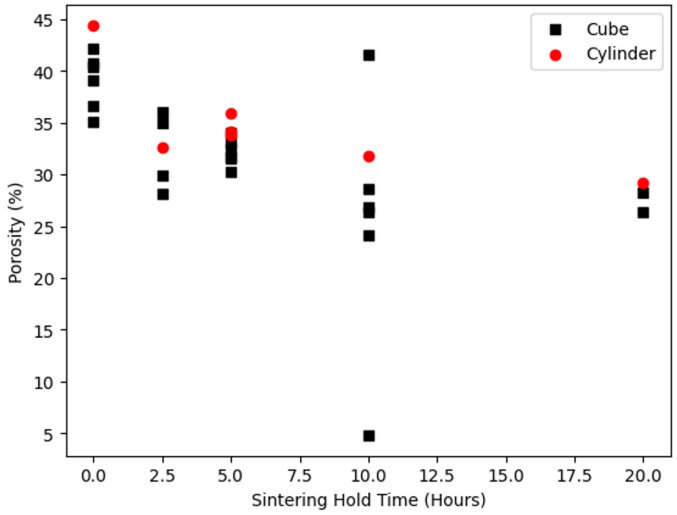

Fig. 3. Porosity as a function of sintering hold time.

From Fig. ***3*** it appears that both the cylinders and cubes follow the same trend in terms of porosity. However, the cylinders did tend to produce porosity values slightly higher than that of the cubes but not by a significant value. The reason for the slight increase in porosity is likely caused by distortion of occurring within the part due to gas buildup causing cavities/delamination to form inside the sample, resulting in macro pores that can be seen with the naked eye, shown in Fig. ***4***. The larger size of the cylinders likely caused the higher levels of distortion, increasing the chance of trapped gases.

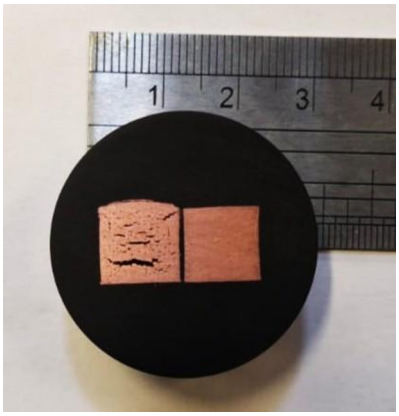

Fig. 4. A cross-section of one of the samples

Fig. ***5*** below shows a microscopic image of a sample interior. The areas in black are empty space while the areas in white show solid material. The structure below is present through the entire structure of the sample and explains the reason for the porosity found, even in samples without any visible macropores of the type seen in Fig. ***4***, due to the presence of micropores as a result of the loss of binder, and the spherical copper particles not being able to form a solid mass after fusing during sintering, due to their geometry. These two categories of voids cause the porosity seen.

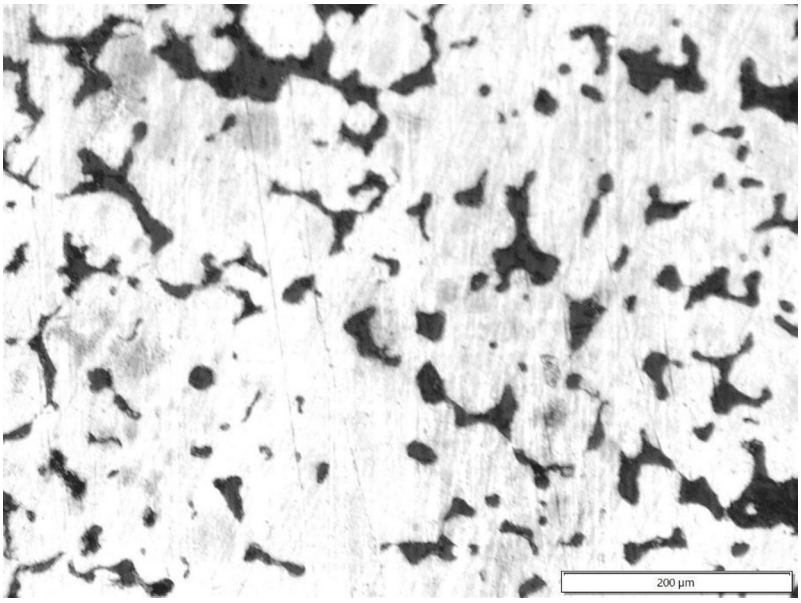

Fig. 5. A microscopic image of a sample test.

The most likely explanation for why sintering hold-time influences porosity is that leaving the samples in an environment where the temperature is close to the samples melting point causes the internal porosity to begin to close [25]. Therefore, is porosity more closely approximating a solid sample. It stands to reason that maximum porosity can be achieved at a hold time of 0 hours and a minimum porosity can be achieved with a hold time of 10 hours.

Both density and volume loss are directly linked to the porosity, as both are simply inverses of the porosity curve ranging from 5000-7000 kg/m^3 and 35 to 5 % respectively. Mass loss on the other hand remained relatively constant across all sintering hold times at 8.5%.

3.2 Specific heat capacity

The specific heat capacity of the samples was in the range of 340-400 J/kgK which is significantly lower than the anticipated value being 390 J/kgK [26]. It was found that this property is not a strong function of sintering hold time and based on Fig. ***6***. It appears to be somewhat random or a function of a currently unknown valuable.

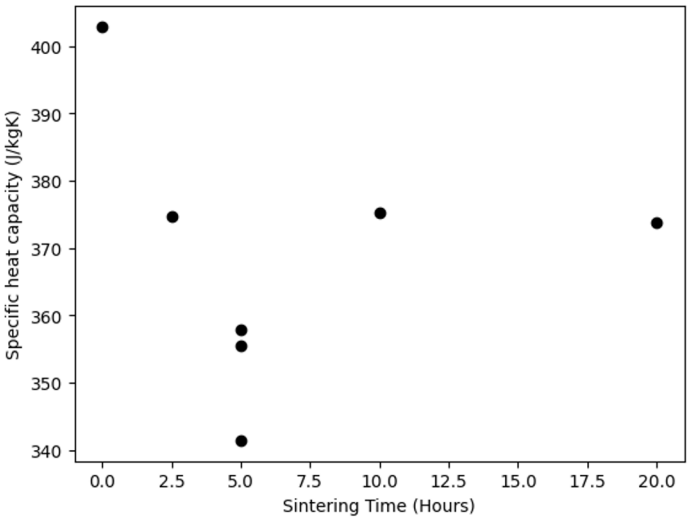

Fig. 6. The specific heat capacity as a function of sintering time for the cylindrical samples.

It is unclear at this time what has caused the specific heat capacity of the samples to be below the anticipated value, but it is likely caused by impurities in the samples that arose during sintering. There was also one measurement that produced a value higher than the anticipated specific heat capacity since only one measurement produced this value it is likely an outlier.

Additionally, all samples (especially samples with a sintering hold time of 0 hours) produced smoke when heated above 150 C^o which implies the presence of impurities. As it currently stands this black material and impurities are the most likely explanation for the reduced specific heat capacity. However, without a full chemical analysis being performed on samples a conclusive finding is impossible to determine.

3.3 Thermal conductivity

As can be seen in Fig. *7* the sintering process has significantly reduced the thermal conductivity of the copper samples. With copper having a baseline thermal conductivity of 390 W/mK [26] the sintering process has resulted in roughly a 80% reduction in thermal conductivity. It can be also seen that thermal conductivity appears to be a function of porosity

and by extension sintering hold time. With increased porosity resulting in reduced thermal conductivity. This is an expected result since increased porosity implies a decrease in the effective contact surface area within the sample. Additionally, the porous structure results in a more complex path for heat to travel. This reduces effective thermal conductivity.

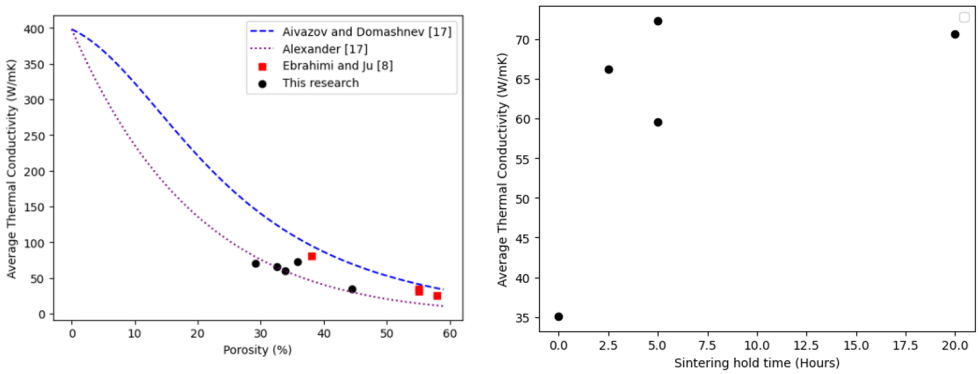

(a) (b)

Fig. 7. Relationship between thermal conductivity and porosity from experimental results relative to modeled data (a), thermal conductivity as a function of sintering hold time (b).

Based on Fig. *7* (b) samples subjected to a sintering hold time of 0 hours resulted in the lowest thermal conductivity of approximately 35 W/mK. While a sintering hold time of 5 hours resulted in the highest thermal conductivity of approximately 73 W/mK. Again, much like porosity, thermal conductivity appears to follow a somewhat exponential pattern. However, increasing sintering hold time only improves the thermal conductivity to a point (roughly 70 W/mK).

The reason for the change in thermal conductivity as a function of sintering hold time is most likely caused by porosity and contamination reduction. It was noted in the porosity discussion that porosity decreases to a point as the sintering hold time increases. By extension this is likely to cause a lot of macro and micro pores within the sample to begin to shrink in size thus producing a more solid component. This seems to be further corroborated by the density results as density also appeared to increase as sintering hold time increases. Additionally, it was noted that during testing the samples with an increased sintering hold time, greater than 10 hours; did not produce smoke when heated above 150 C^{o}. This implies a possible reduction in the formation of impurities. However, without full chemical analysis this point cannot be confirmed and should be treated as a preliminary finding.

When comparing the thermal conductivity to previous research done by Ebrahimi and Ju [8] which is also shown on Fig. *7* (a) it can be seen that the thermal conductivity of this research appears to be slightly lower than that of previous research. However, both sets of data appear to follow a similar trend. The most likely explanation for why this study's findings differ from Ebrahimi and Ju [8] is that they used a shorter sintering hold time as well as a reduced sintering temperature in their study. Based on the data from their study this has caused a slight increase in comparable thermal conductivity values.

A likely explanation for the large drop in thermal conductivity is porosity and contamination. While the presence of contamination within the sintered parts has not been

proven in this research, it was noted in the specific heat capacity discussion that a black surface forms on the parts during sintering both internally and externally this contamination could potentially be causing diffusion barriers preventing effective heat transfer. However, without a full chemical analysis of the samples it is impossible to determine the composition of the contamination or effects. However, it is extremely likely that this contamination is a combination of some form of oxidation and chemical byproducts of the sintering such as carbon. This finding was also observed in Ebrahimi and Ju [8] study. Thermal conductivity was also noted as being a thermal property that is particularly sensitive to the internal structure of the material [16, 27]. Due to this dependency porosity would have a large impact on the thermal conductivity this finding was also noted by Ebrahimi and Ju [8].

Additionally, Fig. *7* (a) presents two empirical models for estimating the thermal conductivity as a function of porosity. The models are models constructed by Alexander [27] and Aivazov and Domashnev [27]. In general, the thermal conductivity values range between these two models with the data from this research conforming somewhat well to the Alexander model. Therefore at least for the samples used in this research the Alexander model shown in equation (7) below can be used to estimate the thermal conductivity of samples prior to sintering.

$$k_{sample} = k_{fluid}\left(\frac{k_{solid}}{k_{fluid}}\right)^{(1-\emptyset)^{\varepsilon}} \tag{7}$$

- k_{solid}: Thermal conductivity of the material if it was not porous ($\frac{k}{mK}$)
- k_{fluid}: Thermal conductivity of the working fluid that the sample is submerged ($\frac{k}{mK}$). In this case air.
- $\emptyset$: Porosity expressed as a dimensionless number
- ε: Experimental constant set to 0.53 [27].

In terms of what has caused the reduced thermal conductivity, it is most likely to be caused by porosity or impurities. Much like specific heat capacity thermal conductivity is a material property and is inherent to a given material and its chemical composition. However, due to the nature of the experiment used in this study the effective thermal conductivity is what was actually measured. Effective thermal conductivity can be swayed by many factors, but it's generally swayed by thermal resistance. Based on the information available it seems likely that the effective thermal conductivity of the samples has largely been influenced by the porosity. However, there's also the possibility that the internal chemical composition of the samples themselves has been altered. However, without a full chemical analysis as with specific heat capacity this is impossible to determine definitively.

4 Conclusions

This research attempted to characterize the material properties of additively manufactured parts. From this research the following conclusions can be made.

- Porosity is a function of sintering hold-time and has a lower limit of roughly 25% and an upper limit of 43% for the bound powder extrusion method employed

- Density is the inverse of the porosity with a lower limit of 5000 kg/m^3 and an upper limit of 7000 kg/m^3, which is 56 and 79 % of the base material.
- The average mass loss during sintering was 8.5%.
- Specific heat capacity ranges from 340-400 J/kgK, 87-102 % of the base material.
- Thermal conductivity is a function of sintering hold time and appears to be lower than previous research, with an upper limit of roughly 73 W/mK and a lower limit of 35 W/mK, which is 19 and 9% of the base material.
- The Alexander model [27] model can be used to estimate the thermal conductivity based on porosity with an average error of within 13 %.

Finally, it is recommended that research be continued into understanding the thermal conductivity and specific heat capacity, with special emphasis paid on determining the chemical composition of the sintered samples and oxides layers, as well as understanding how to reduce porosity further.

This work is based on the research supported in part by the National Research Foundation of South Africa Thutuka grant (TTK2204051996) and postgraduate scholarship (PMDS230601112291).

References

1. HUBS. *What is metal 3D printing and how does it work?* 2023 [cited 2023 21 March]; Available from: https://www.hubs.com/knowledge-base/introduction-metal-3d-printing/.
2. Tamás Markovits and Varga L.F., *Investigating the surface roughness of 3D printed metal parts in case of thin 20 μm build layer thickness.* Journal of Materials Research 2024. **39**: p. 10.
3. W.M. Rohsenow, Hartnett J.P., and Ch Y.I., *Handbook of heat transfer*. 3 ed. 1998, New York: McGraw-Hill.
4. Y. Cengel and Ghajar A., *Heat and Mass Transfer: Fundamentals and Applications*. 6 ed. 2020: McGraw Hill.
5. Markforged. *Types of 3D Printing in Metal*. n.d. [cited 2024 25 March]; Available from: https://markforged.com/resources/learn/design-for-additive-manufacturing-metals/metal-additive-manufacturing-introduction/types-of-3d-printing-metal.
6. The Virtual Foundry. *Getting Your Own Custom 3D Printing Filament*. 2022 [cited 2023 21 March]; Available from: https://thevirtualfoundry.com/wp-content/uploads/2022/01/Getting_Your_Own_Custom_3D_Printing_Filament.pdf.
7. The Editors of Encyclopædia Britannica. *Bronze*. 2024 [cited 2024 18 Feburary]; Available from: https://www.britannica.com/technology/bronze-alloy.
8. N.D. Ebrahimi and Ju Y.S. *Thermal conductivity of sintered copper samples prepared using 3D printing-compatible polymer composite filaments*. 2018 [cited 2024 16 February]; Available from: https://www.sciencedirect.com/science/article/pii/S221486041830575X.
9. B.D. Bock, Pretorius K., and Scott S. *3D printing for heat transfer: characterisation of additive manufactured copper*. 2023 [cited 2024 18 Feburary]; Available from: https://www.matec-conferences.org/articles/matecconf/abs/2023/15/matecconf_rapdasa2023_08004/matecconf_rapdasa2023_08004.html.

10. R. Urwin and Bock B.D., *Geometric and hardness characterization of additively manufactured copper using bound powder extrusion with thermal sintering*, in *RAPDASA 2024*. 2024, MATEC: Gqeberha. p. 14.
11. J.E. Montes-Ramirez, et al., *Shrinkage and deformation compensation in metal fused filament fabrication (mf3) sintered copper components using 3d scanning and inverse deformation.* Journal of Manufacturing Processes, 2024. **121**: p. 10.
12. Gurminder Singh and Pandey P.M. *Experimental investigations into mechanical and thermal properties of rapid manufactured copper parts*. 2019 [cited 2024 20 September]; Available from: https://www.researchgate.net/publication/335881134_Experimental_investigations_into_mechanical_and_thermal_properties_of_rapid_manufactured_copper_parts.
13. Thang Q. Tran, et al. *3D Printing of Highly Pure Copper*. 2019 [cited 2024 20 September]; Available from: https://www.mdpi.com/2075-4701/9/7/756.
14. Loic Constantina, et al. *Laser 3D printing of complex copper structures*. 2020 [cited 2024 20 September]; Available from: https://www.sciencedirect.com/science/article/pii/S2214860420306400.
15. L.C. Wei, et al. *Thermal conductivity of metal powders for powder bed additive manufacturing*. 2018 [cited 2025 22 May]; Available from: https://www.sciencedirect.com/science/article/pii/S2214860417306231.
16. C. Vincent, et al. *Effect of porosity on the thermal conductivity of copper processed by powder metallurgy*. 2012 [cited 2025 22 May]; Available from: https://www.sciencedirect.com/science/article/pii/S0022369711004112.
17. The Virtual Foundry. *The Virtual Foundry - SDS - Copper 24-01*. 2024 [cited 2024 23 May]; Available from: https://thevirtualfoundry.com/wp-content/uploads/2024/03/The-Virtual-Foundry-SDS-Copper-24-01.pdf.
18. The Virtual Foundry. *PRINTING PURE METAL WITH FILAMET™*. 2023 [cited 2023 23 April]; Available from: https://thevirtualfoundry.com/help/.
19. The Virtual Foundry. *Sintering Carbon (0.5kg)*. 2023 [cited 2023 23 April]; Available from: https://shop.thevirtualfoundry.com/en-za/products/sintering-carbon-0-5kg-1?variant=31189805924435.
20. Merck. *Copper*. n.d. [cited 2024 23 May]; Available from: https://www.merckmillipore.com/ZA/en/product/Copper,MDA_CHEM-102703.
21. Polyfluor Plastics. *PLA Filament*. 2011 [cited 2024 2 June]; Available from: https://www.polyfluor.nl/assets/files/datasheet-pla-filament-uk.pdf.
22. E.J.G. John. A. Slotwinski, and Keith M. Hebenstreit, *Porosity Measurements and Analysis for Metal Additive Manufacturing Process Control.* Research of the National Institute of Standards and Technology, 2014. **119**.
23. BIPM, et al., *Evaluation of measurement data — Guide to the expression of uncertainty in measurement*. First ed. JCGM 100:2008 GUM 1995 with minor corrections. 2008.
24. I. Marifatin and Muntini M.S. *The Measurement of Thermal Conductivity with Comparative Methods For Thermolectric Materials*. 2023 [cited 2025 8 May]; Available from: https://www.researchgate.net/publication/377068716_The_Measurement_of_Thermal_Conductivity_with_Comparative_Methods_For_Thermolectric_Materials.
25. M.A. Almomani, Shatnawi A.M., and Alrashdan M.K., *Effect of Sintering Time on the Density, Porosity Content and Microstructure of Copper – 1 wt. % Silicon Carbide Composites.* 2014. **1064**: p. 5.
26. MATWEB. *Copper, Cu; Annealed*. [cited 2024 2 February]; Available from: https://www.matweb.com/search/datasheet_print.aspx?matguid=9aebe83845c04c1db5126fada6f76f7e.

27. O. Biceroglu, et al., *THERMAL CONDUCTIVITY OF SINTERED METAL POWDERS AT ROOM TEMPERATURE.* HEAT AND MASS TRANSFER, 1976. **3**: p. 9.